

Supplementary Information for

Bessel-beam-based side-view measurement of seven-core fibre internal core distribution

Liuwei Zhan¹, Runze Zhu¹, Hongwei Tong¹, Haogong Feng¹, Kanghu Zhou¹,
and Fei Xu^{1, *}

¹ College of Engineering and Applied Sciences and Collaborative Innovation Centre of Advanced Microstructures, Nanjing University, Nanjing 210093, Jiangsu Province, China.

*feixu@nju.edu.cn

1 Results of changing fibre sizes and core numbers

Based on the commercial seven-core fibre (YOFC, 150um diameter), different diameters of fibre (100um and 150um) and different core numbers of fibre (4-core and 10-core) were obtained for simulation to verify that changing fibre size or core number is also suitable for clearly imaging the fibre core based on the Bessel beam illumination method. It should be noted that only the parameters of the fibre were changed, and the other parts in the optical path remained unchanged. Fig. S1, Fig. S2, and Fig. S3 show a higher-contrast transmission pattern when using the Bessel beam as the illumination light, which provides a clearer pattern for core distribution measurement.

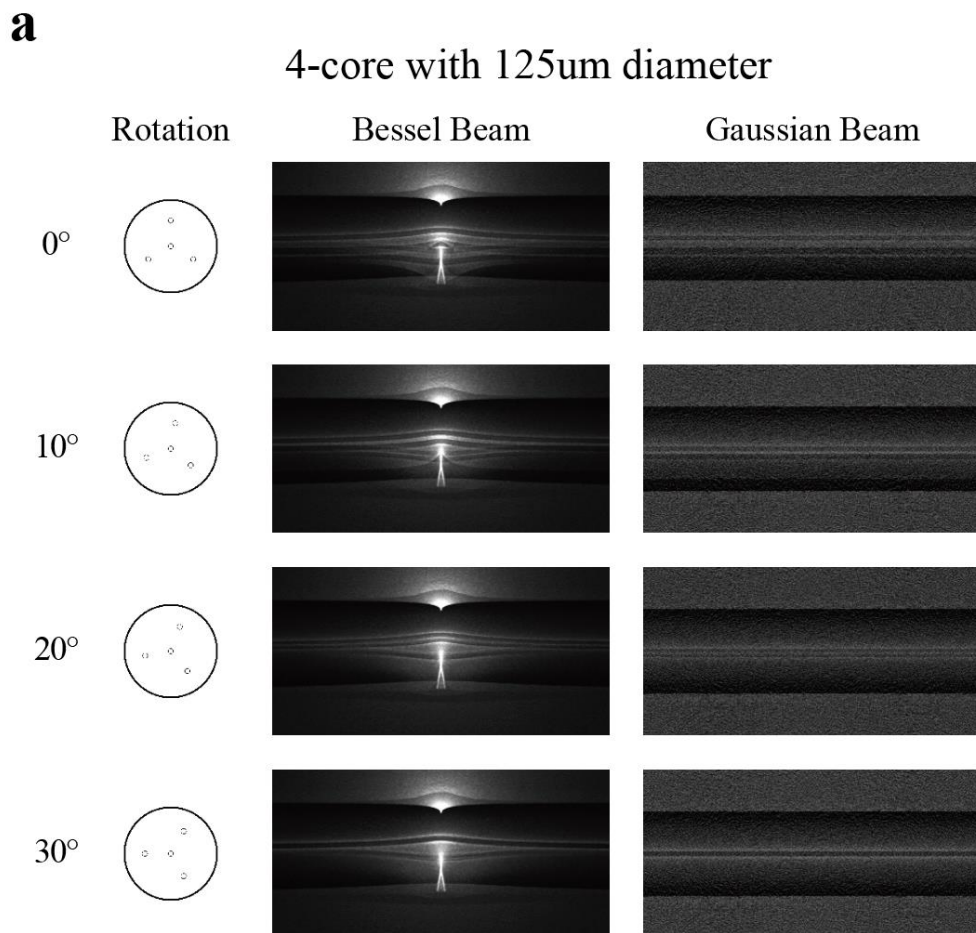


Fig. S1. Pattern comparison of 4-core fibre with a diameter of 125um under the illumination conditions of Bessel beam and Gaussian beam. a The 4-core fibre with a diameter of 125um is simulated with fibre rotation of 0°, 10°, 20°, and 30°.

a

4-core with 150um diameter

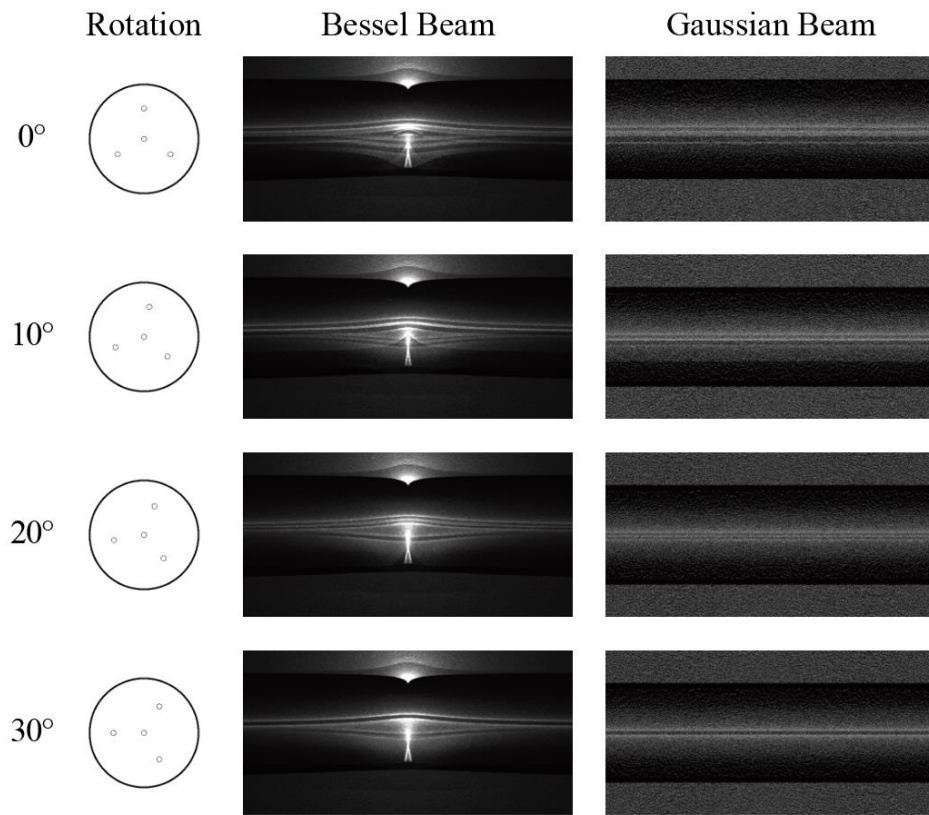


Fig. S2. Pattern comparison of 4-core fibre with a diameter of 150um under the illumination conditions of Bessel beam and Gaussian beam. a The 4-core fibre with a diameter of 150um is simulated with fibre rotation of 0°, 10°, 20°, and 30°.

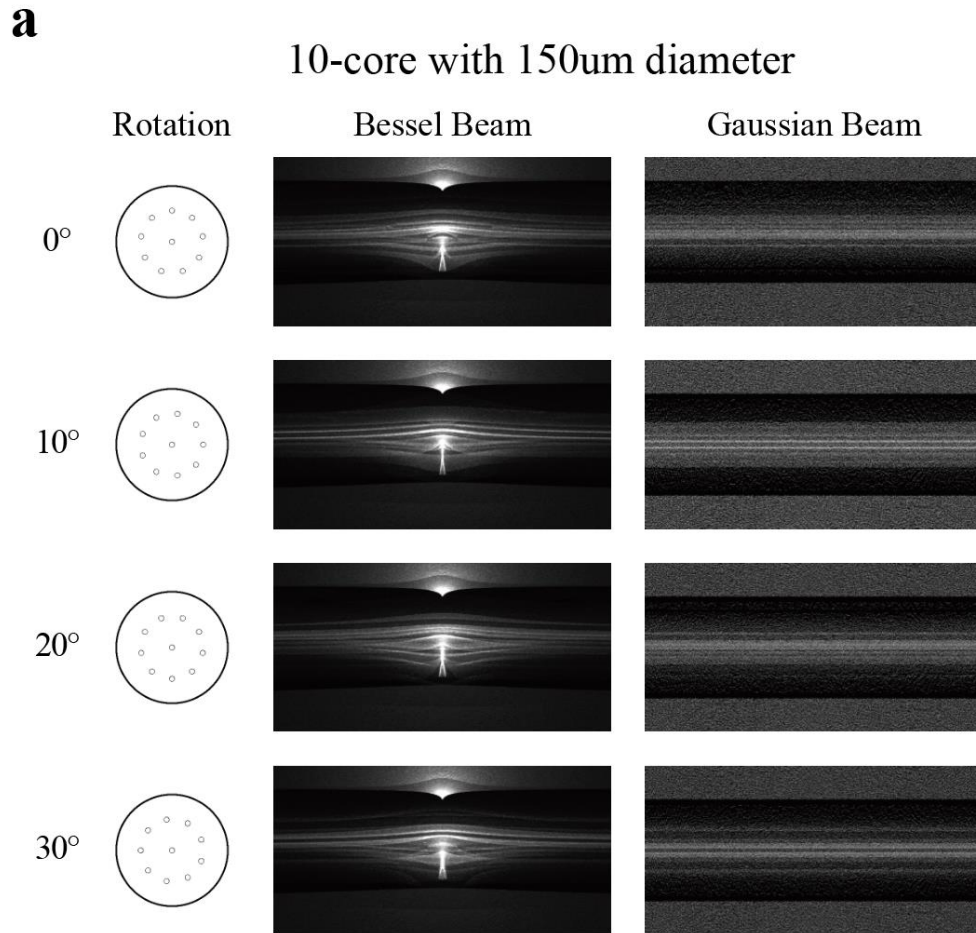


Fig. S3. Pattern comparison of 10-core fibre with a diameter of 150um under the illumination conditions of Bessel beam and Gaussian beam. a The 10-core fibre with a diameter of 150um is simulated with fibre rotation of 0°, 10°, 20°, and 30°.

2 Comparison between fibres with different diameters

Based on the actual seven-core fibre (YOFC, 150um diameter), different diameters of fibre (100um, 450um) was obtained by scaling equally for simulation to verify that under the illumination conditions of using the same optical components, different cores can still be clearly distinguished in the pattern of Bessel beam transmitted through the fibre, as shown in Fig. S4.

a

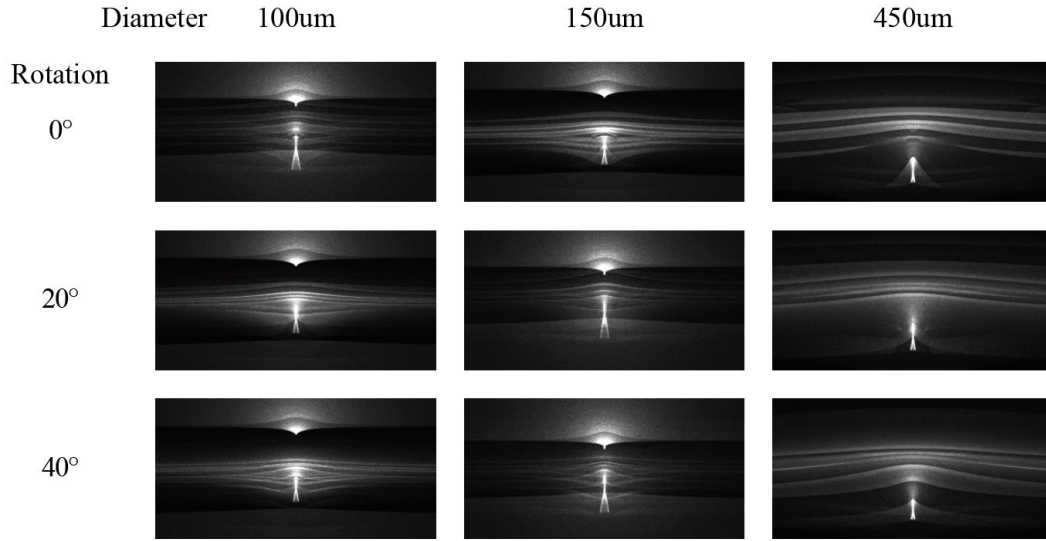


Fig. S4. Comparison between fibres with different diameters in simulation. a The seven-core fibre with diameters of 100um, 150um, and 450um are simulated with fibre rotation of 0°, 20°, and 40°, showing that fibres of different diameters can have good results separating different cores under the same illumination source.

3 Precision calculation

The precision of the core distribution measurement was defined as the width of the core distribution when the correlation coefficient drops to $\frac{-1dB}{50}$ of the peak. As shown in Fig. S5, the peak correlation coefficient is 0.933966 for the Bessel beam and 0.985017 for the Gaussian beam when the measured pattern is 0°. The width of the core distribution of -1dB of the peak in reference patterns is 9.9875° of the Bessel beam and 25.568° of the Gaussian beam. Similarly, when the measured pattern is 20° and 40°, the width is 5.6929° and 9.1883° of Bessel beam, and 18.2771° and 16.4791° of Gaussian beam. The precision of 0.166° and 0.402° is then obtained by averaging the width of the core distribution of three measured patterns and dividing by 50.

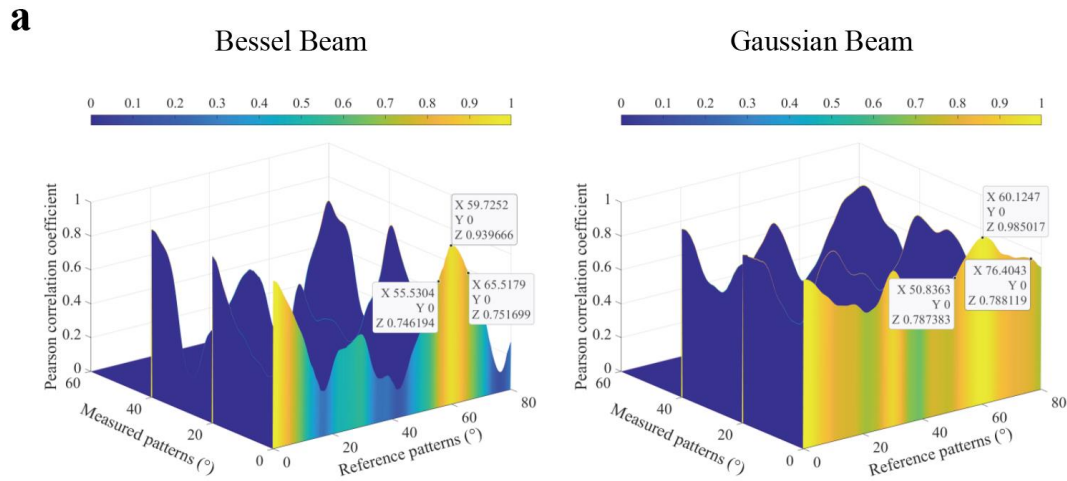


Fig. S5. Calculation of precision of the core distribution measurement. **a** The coordinate points on both sides of the peak are the position when the peak drops by -1dB.

4 Deep learning data pre-process

In this study, an automated rotation-capture-rotation image capture cycle was achieved with the aid of the rotation apparatus and self-developed software. The cyclic process involves rotating the seven-core fibre and acquiring a Bessel beam transmission image, as well as an image of the fibre end-face image to measure the fibre core angle distribution. As the fibre cores are arranged equidistantly based on the vertices and centres of the hexagon, identifying the angle can be simplified to 0–60 degrees. The transmission images were marked with the angle through the process, as shown in Fig. 4a.

To process the acquired raw image, the software first cropped the image to remove the extra black margins surrounding the fibre end-face. Subsequently, the contour curves of the seven circular fibre cores were obtained using graphical processing techniques, such as grayscale, threshold binarization, and edge detection. Finally, the centre coordinates of the circles were calculated using a fitting function, and the angle of the fibre core angle distribution was determined by utilizing trigonometric functions. With this method, an efficient and reliable tool was developed to acquire multicore fibre transmission images and mark core angle distributions in an automated manner.

5 Neural network structure

In the study, a Convolutional Neural Networks-based (CNN) approach for fibre core angle distribution recognition is employed, with an image classification task. The base CNN model utilized in the study is the ConvNeXt neural network, which is a modified version of the ResNet network. The structure of the ConvNeXt network is shown in Fig. S6, and it is similar to ResNet in that both models extract image features through the stacking of residual blocks with different feature layer lengths. After multi-layer feature extraction, a Global Average Pooling (G.A.P) layer is applied to the data to minimize overfitting by reducing the total number of parameters in the model. Subsequently, the normalization layer and the Softmax layer are used to map the two-dimensional feature data to the one-dimensional predicted classification. Data is labelled using one-hot encoding.

The network structures used for deep learning are large and have many parameters that require a GPU to accelerate the computation, so in the training step, it requires workstation computers with powerful GPUs. Also, since training a large network requires a lot of samples, it takes some preparation time. However, once the network training is complete, the trained network can be transferred to a dedicated GPU, NPU or FPGA that can be adapted to edge computing, which is portable and inexpensive.

A database of Bessel beam transmission patterns with core angle distributions saved at angle resolutions of 0.2° was created, corresponding to 300 classification categories (by one-hot encoding). To account for potential image discrepancies caused by platform micro-vibrations, multiple photos were captured for each classification category.

The dataset is derived from the pattern of the Bessel beam transmitting through a seven-core fibre at different core angle distributions, captured by CMOS. To reduce redundancy information, the original images were cropped to retain only the central 500×500 pixels and then resized to 224×224 pixels to accelerate the training process. In the training dataset consisting of images captured by 15 fibres, 20% images were randomly selected as validation dataset, which are not involved in network training,

and the validation dataset were used to evaluate the classification performance of the neural network after each training epoch. The cross-entropy loss function, commonly utilized in multi-classification tasks, was employed in this study

$$Loss = -\frac{1}{n} \sum_{i=1}^n y_i \log \hat{y}_i \quad (1)$$

Here, y_i represents the true category value of the sample, \hat{y}_i denotes the predicted value from the neural network, and n is the number of classification categories. As the distribution of the predicted sample \hat{y}_i gets closer to the true value y_i , $Loss$ becomes smaller until it approaches zero.

The model was trained on a computer with an AMD Ryzen 5600X processor, 32GB RAM, and an NVIDIA GeForce GTX 1660 SUPER graphics card, using the PyTorch environment. The batch size was set to 8, and the learning rate was initially set to $5e-4$, with AdamW used as the optimizer. To achieve faster and more accurate model convergence, the learning rate decreased as the training epoch increased.

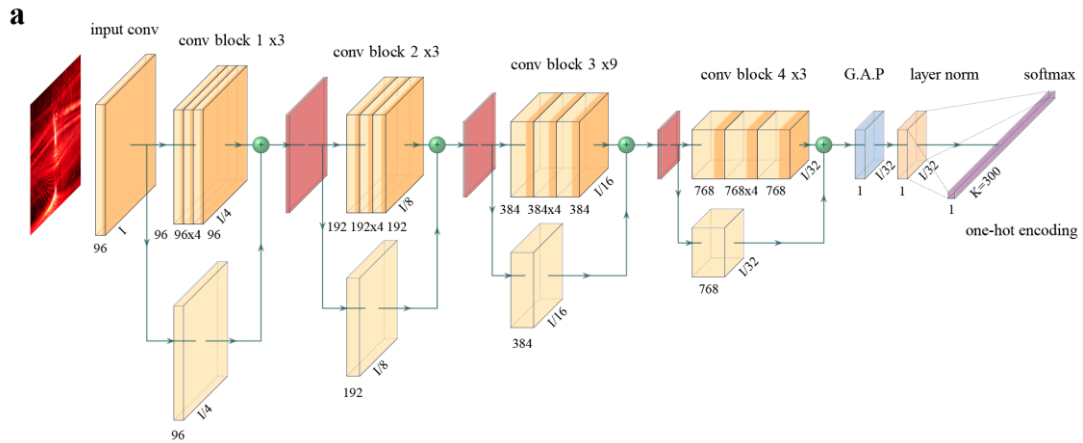


Fig. S6. Deep learning neural network structure. a The structure of the Convolutional Neural Network of ConvNeXt. Ultra-deep neural networks are formed by combining multi-scale residual blocks.